Cell

Enhanced Polyubiquitination of Shank3 and NMDA Receptor in a Mouse Model of Autism

M. Ali Bangash,[1] Joo Min Park,[1,6] Tatiana Melnikova,[2,6] Dehua Wang,[4,6] Soo Kyeong Jeon,[1] Deidre Lee,[2] Sbaa Syeda,[2] Juno Kim,[1] Mehreen Kouser,[3] Joshua Schwartz,[1] Yiyuan Cui,[4] Xia Zhao,[4] Haley E. Speed,[3] Sara E. Kee,[3] Jian Cheng Tu,[1] Jia-Hua Hu,[1] Ronald S. Petralia,[5] David J. Linden,[1] Craig M. Powell,[3] Alena Savonenko,[2] Bo Xiao,[1,4] and Paul F. Worley[1,*]
[1]Department of Neuroscience
[2]Departments of Pathology and Neurology
Johns Hopkins University School of Medicine, Baltimore, MD 21205, USA
[3]Departments of Neurology and Psychiatry, The University of Texas Southwestern Medical Center, Dallas, TX 75390-8813, USA
[4]The State Key Laboratory of Bio-Therapy, West China Hospital, Sichuan University, Chengdu 610065, China
[5]Laboratory of Neurochemistry, National Institute on Deafness and Other Communication Disorders, National Institutes of Health, Bethesda, MD 20892, USA
[6]These authors contributed equally to the work
*Correspondence: pworley@jhmi.edu
DOI 10.1016/j.cell.2011.03.052

SUMMARY

We have created a mouse genetic model that mimics a human mutation of Shank3 that deletes the C terminus and is associated with autism. Expressed as a single copy [Shank3(+/ΔC) mice], Shank3ΔC protein interacts with the wild-type (WT) gene product and results in >90% reduction of Shank3 at synapses. This "gain-of-function" phenotype is linked to increased polyubiquitination of WT Shank3 and its redistribution into proteasomes. Similarly, the NR1 subunit of the NMDA receptor is reduced at synapses with increased polyubiquitination. Assays of postsynaptic density proteins, spine morphology, and synapse number are unchanged in Shank3(+/ΔC) mice, but the amplitude of NMDAR responses is reduced together with reduced NMDAR-dependent LTP and LTD. Reciprocally, mGluR-dependent LTD is markedly enhanced. Shank3(+/ΔC) mice show behavioral deficits suggestive of autism and reduced NMDA receptor function. These studies reveal a mechanism distinct from haploinsufficiency by which mutations of Shank3 can evoke an autism-like disorder.

INTRODUCTION

Autism represents a broad spectrum of behavioral and cognitive disorders characterized by early onset deficit of language development and social interactions, accompanied by repetitive behaviors. Most cases of autism spectrum disorders (ASD) are sporadic and cannot yet be linked to mutations of specific genes. Nevertheless, a significant fraction of ASD is caused by de novo or rare mutations (Geschwind, 2008). One of the most commonly associated genetic conditions is fragile X mental retardation syndrome in which 30% of patients show symptoms of ASD. Mouse models that delete the *Fmr1* gene show changes in synaptic plasticity; especially enhanced mGluR evoked long-term depression, which has been linked to cognitive deficits (Huber et al., 2002). Another ASD-linked mutation involves the *Shank3* gene, also called ProSAP1/CortBP1. *Shank3* is located on chromosome 22q13.3 in humans and was first implicated in ASD associated with the 22q13.3 microdeletion syndrome (also known as the Phelen-McDermid Syndrome) characterized by dysmorphic facial features, delayed expressive speech, and autistic behavior (Nesslinger et al., 1994). Subsequent genetic analysis of patients with chromosome 22q13.3 deletion syndrome revealed a balanced translocation of chromosomes 12 and 22 causing a disruption of *Shank3* gene at exon 21, implicating the haploinsufficiency of *Shank3* gene as a causal mechanism (Bonaglia et al., 2001). More recently, heterozygous mutations in *Shank3* gene have been shown to cause ASD in a gene-dosage-dependent manner (Durand et al., 2007; Moessner et al., 2007). ASD cases with *Shank3* mutations range from severe cases of autistic disorder to milder variants with Asperger syndrome (Durand et al., 2007). Genome-wide association studies confirm the link between *Shank3* mutations and ASD (Marshall et al., 2008; Sebat et al., 2007). Additionally, a Shank3 mutation is reported in association with schizophrenia (Gauthier et al., 2010).

Shank proteins are products of three related genes, *Shank1–Shank3,* and are expressed as a number of spliced variants. Shank proteins include 5–6 N-terminal ankyrin repeats followed by a well-conserved SH3 (Src homology 3) domain, a PDZ (PSD95/Discs large/zona-occludens-1) domain, a proline-rich domain, and a C-terminal SAM (sterile alpha motif) domain. Homer proteins bind Shank to create a polymeric network structure that is dependent on Homer tetramerization, as well as physical interactions between Shank proteins (Hayashi et al., 2009). Human genetic studies point toward a possible role of Shank3-Homer interaction in ASD. The balanced translocation of chromosomes 12 and 22 causes a disruption of exon

21, which encodes the Homer-binding site (Bonaglia et al., 2001). A second instance involves two siblings heterozygous for a guanine insertion in exon 21, creating a frameshift and a truncated Shank3 protein lacking the Homer-binding site (Durand et al., 2007). Point mutations elsewhere in *Shank3*, for instance within the ankyrin repeats, are also associated with ASD but are typically less severe than mutations with loss of the Homer-binding domain (Durand et al., 2007).

To examine the importance of Shank3-Homer interaction in the pathogenesis of ASD, we generated a mouse model of Shank3 that deletes the Homer-binding domain at the C terminus (ΔC), thus mimicking the reported mutation in ASD patients (Durand et al., 2007). Here we report that the heterozygous ΔC Shank3 mutation results in a striking downregulation of wild-type (WT) Shank3. This downregulation of Shank3 is not consistent with a simple gene-dosage model because Shank3 at excitatory synapses is reduced >90%. Instead, we find an increase in WT Shank3 that is polyubiquitinated and relocalized to proteasomes. This effect appears highly specific to Shank3 given that Shank3ΔC does not result in downregulation of Shank1, Shank2, GKAP, AMPA type glutamate receptors, or most other synaptic proteins. The notable exception is the NR1 subunit of the NMDA receptor (NMDAR), which is downregulated at synapses in association with increased polyubiquitination. Assays of synaptic morphology and synapse number do not reveal differences between adult WT and Shank3(ΔC) mice. However, electrophysiological studies confirm a reduction of NMDAR responses in cortical and hippocampal neurons and reduced NMDAR-dependent long-term potentiation (LTP) and long-term depression (LTD). Moreover, the amplitude of mGluR-LTD is increased in the hippocampi of Shank3(+/ΔC) mice. Studies of Shank3(ΔC) mice in behavioral assays reveal deficits of social interaction, consistent with ASD. Additionally, Shank3(+/ΔC) mice show enhanced locomotor responses to amphetamine and the NMDA antagonist MK-801, consistent with the reduction of NMDAR function and similar to "schizophrenia-like" symptoms reported in mouse models with reduced NR1 expression (Mohn et al., 1999). Our studies reveal a molecular pathway that may underlie neurodevelopmental disorders linked to human mutations of Shank3.

RESULTS

Generation of the ΔC Shank3 Mouse

To determine how Homer affects Shank3 expression in vivo, we examined Homer-triple knockout (HTKO) mice for Shank3 levels. These mice lack all Homer (1, 2, 3, and 1a) isoforms. We found an 80% reduction in Shank3 in cortical lysates using three independent Shank3 antibodies (Figures S1A and S1B available online). Shank1 and 2 isoforms, which also bind Homer, were reduced ~50%. Similarly, cortical cultures from the HTKO mice showed ~80% reduction in Shank3 as measured by immunohistochemistry (Figures S1C–S1E). Single Homer1 KO mice had ~40% reduction in Shank3 (Figure S1F). We were able to rescue the reduction in Shank3 levels in the HTKO cultures by transiently expressing full-length Homer1c isoform (Figure S1G), but not point mutants of Homer1c (W24A and G89N) that do not bind Shank3 (Beneken et al., 2000), suggesting that the physical association of Homer with Shank3 is necessary to maintain Shank3 levels. We found no evidence of changes in Shank3 mRNA in the HTKO brains (Figure S1H). These data support the notion that Homer stabilizes Shank3 protein in vivo.

Given the reduction of Shank3 in the Homer TKO and the importance of Shank3 in ASD, we generated a mouse that affords conditional deletion of exon 21 of *Shank3* (Figure S1I). Excision of exon 21 creates a frameshift such that the resulting Shank3 protein (termed ShankΔC) is predicted to lack the entire C-terminal portion of Shank3, including the Homer-binding site in the proline-rich domain and the SAM domain (Figure S1K). We confirmed excision of exon 21 in a cross with a mouse expressing actin-Cre (Figure S1J) and evaluated expression of Shank3 proteins using N- and C-terminal targeted Shank3 antibodies reacted with cortical lysates from WT Shank3(+/+), Shank3(+/ΔC), and Shank3(ΔC/ΔC) mice (Figure 1A). Both the C-terminal antibodies (JH3025 and H160) reacted with two prominent bands (~190 and ~120 kDa) that are absent in Shank3(ΔC/ΔC), indicating that they specifically detect Shank3. The N-terminal Shank3 antibody reacted with a single band that is the same apparent molecular weight (MW) as the largest band detected by the C-terminal antibody and is absent in Shank3(ΔC/ΔC). Additionally the N-terminal antibody (Ab) reacted with an ~90 kDa band that is present in Shank(ΔC/ΔC) and Shank(+/ΔC) but absent in Shank3(+/+) (Figure 1A). These studies confirm the specificity of antibodies and demonstrate expression of mutant Shank3ΔC protein in brain.

Gain-of-Function Reduction of WT Shank3 in the Shank3(+/ΔC) Mouse

Because Shank3 mutations in humans are associated with ASD in a heterozygote genotype (Durand et al., 2007), we decided to analyze the Shank3(+/ΔC) mouse. Shank3(+/ΔC) mice were born with expected Mendelian frequency and appeared healthy and of normal size through development and into adulthood. Biochemical analysis, with three independent Shank3-specific antibodies (JH3025, H160, and N-term), of the Shank3(+/ΔC) cortical lysates of 8-week-old mice revealed a 70%–80% reduction in Shank3 protein levels (Figures 1B and 1C). We also assessed Shank3 levels in days in vitro (DIV) 14–21 cortical cultures made from Shank3(+/ΔC) mice and found a similar 75% reduction in Shank3 with no change in PSD-95 or Vglut1 (Figures 1D and 1E). The measured loss of Shank3 in the Shank3(+/ΔC) cultures increased to 90% when we assayed in synaptic fractions (Figure 1F), suggesting that Shank3 at the synapse is preferentially downregulated. We did not observe changes in other Shank isoforms (Shank1 and 2) or other scaffolding molecules GKAP, PSD-95, Homer, and Neuroligin-3 in cortical lysates (Figures 1B and 1C). However, we did detect ~50% reduction in NMDAR subunit NR1 levels in the Shank3(+/ΔC) cortex without significant changes in NR2A, NR2B, AMPA (GluR1), or mGluR5 (Figures 1B and 1C). Shank3 mRNA in Shank3(+/ΔC) brains was ~90% that of Shank3(+/+) (Figure 1G), likely representing compensation from the WT allele. This indicates that the downregulation of Shank3 protein in Shank3(+/ΔC) is not due to a commensurate reduction of Shank3 mRNA.

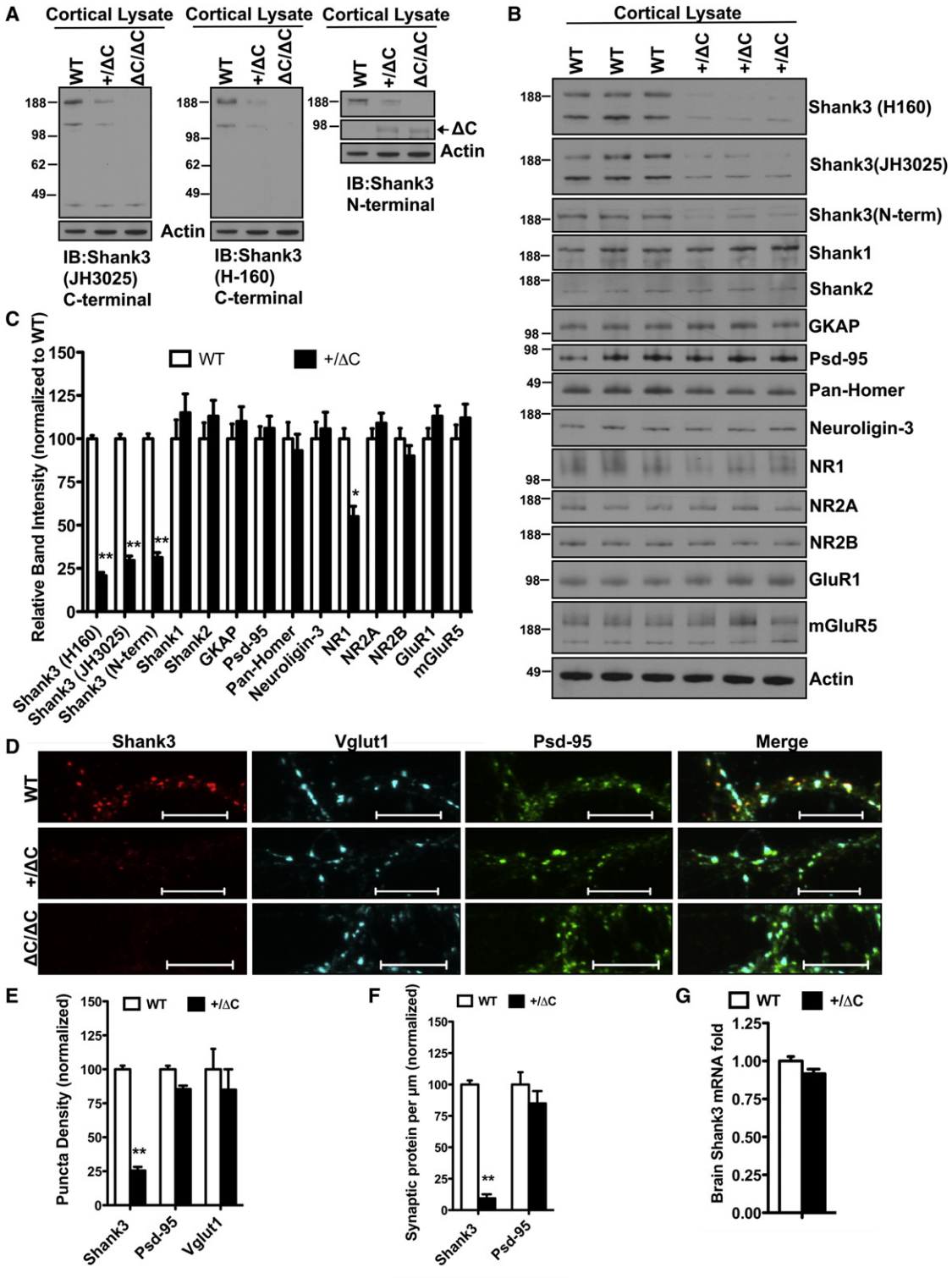

Figure 1. Gain-of-Function Reduction of Shank3 in the Shank3(+/ΔC) Mice

(A) Representative immunoblots from cortical lysates blotted with JH3025 C-terminal antibody (Ab), H-160 C-terminal Ab, and an N-terminal Ab against Shank3. Multiple bands represent spliced Shank3 variants. Lysates from ΔC/ΔC mouse served as negative control. JH3025 gives a nonspecific band ~45 kDa. Actin is used as loading control. See also Figure S1J.

(B) Representative immunoblots from cortical lysates of three independent littermate pairs of WT and Shank3(+/ΔC) mice aged P60.

(C) Quantification of protein levels in (A). n = 3 littermate pairs; $^{**}p < 0.01$; $^{*}p < 0.05$.

Increased In Vivo Polyubiquitination of WT Shank3 in the Shank3(+/ΔC) Mouse

We examined the notion that reduced expression of WT Shank3 in the Shank3(+/ΔC) mouse might be linked to enhanced ubiquitination, as Shank proteins have been reported to be ubiquitinated (Ehlers, 2003). Wild-type Shank3 was immunoprecipitated from cortical lysates with C-terminal Ab and assayed for polyubiquitination using the FK1 Ab (Figure 2A). A 2-fold increase in polyubiquitinated Shank3 was evident in the Shank3(+/ΔC) mouse (Figure 2B). Because polyubiquitination can be a signal for proteasomal degradation, we examined colocalization of WT Shank3 with a proteasomal marker Rpt6 in cortical cultures and detected a 2.5-fold increase in Shank3 puncta colocalizing with Rpt6 in cultures from the Shank3(+/ΔC) mice (Figures 2C and 2D). These findings suggest that the increased polyubiquitination of Shank3 results in enhanced proteasomal degradation in Shank3(+/ΔC) mice. We found no change in total Rpt6 levels in +/ΔC cortical lysates (Figures 2E and 2F), indicating that there was no global upregulation of the proteasome.

Shank3ΔC protein is expressed in brain of Shank3(+/ΔC) mice (Figure 2G, Input) and coimmunoprecipitates with WT Shank3 in vivo (Figure 2G). Shank3ΔC also coimmunoprecipitated (co-IPed) with WT Shank3 when these proteins were coexpressed in HEK293 cells (data not shown), indicating that Shank3 proteins can physically associate independently of their C-terminal SAM domain. The physical association of Shank3ΔC with WT Shank3 may be important for increased polyubiquitination of Shank3, although this issue will require further analysis. To confirm that Shank3ΔC is causal for enhanced degradation of Shank3, we expressed Shank3ΔC transgene in WT cortical cultures and found a 65% reduction in WT Shank3 (Figures 2H and 2I) and an ~80% reduction in synaptic Shank3 (Figure 2J) with no reduction in Vglut1. We examined the possibility that Shank3ΔC is ubiquitinated using the N-terminal Shank3 Ab for immunoprecipitation but failed to detect ubiquitinated Shank3ΔC (data not shown).

We considered a model in which the disruption of Homer binding to Shank3 might result in its enhanced polyubiquitination. To negate possible effects of Shank3ΔC protein, we examined cortical lysates from Homer TKO and found a 2-fold increase in polyubiquitinated Shank3 (Figures S2A and S2B). Similarly, we found a 2-fold increase in Shank3-Rpt6 colocalization in cortical cultures from the Homer TKO (Figures S2C and S2D). We also looked at the role of the activity-dependent dominant-negative Homer isoform, Homer1a. Overexpression of Homer1a in cortical cultures resulted in 50% reduction of Shank3 (Figures S2E and S2F), whereas the Homer1a KO mouse cortex had about a 2.5-fold increase in Shank3 (Figures S2G and S2H) and a concomitant 2-fold reduction in Shank3 polyubiquitination (Figures S2I–S2J). These findings suggest that interruption of Homer binding is sufficient to evoke enhanced proteasomal degradation of Shank3.

NR1 Polyubiquitination Is Increased in the Shank3(+/ΔC) Mice

Our initial observation of NR1 reduction in cortical lysates from Shank3(+/ΔC) mice was verified in cortical synaptoneurosomal (P2) fractions, which showed ~70% reduction in NR1 with no significant changes in NR2A, GluR1, GluR2, or mGluR5 (Figures 3A and 3B). Similarly, we found ~50% reduction in both total and surface NR1 using cortical cultures from Shank3(+/ΔC) mice (Figures 3C–3E). This decrease in NR1 levels could not be explained by a transcription defect because the NR1 mRNA levels were unaltered in the Shank3(+/ΔC) mice compared to WT (Figure 3F). NR1 is reported to undergo ubiquitination (Kato et al., 2005); therefore we assessed whether polyubiquitination of NR1 could underlie the NR1 reduction in the Shank3(+/ΔC) mice. Cortical lysates immunoprecipitated with NR1 and assayed for polyubiquitination using the FK1 antibody (Figure 3G) revealed an ~3-fold increase in polyubiquitinated NR1 in Shank3(+/ΔC) lysates (Figure 3H). Similarly, NR1 expression in HTKO cortex was reduced ~50% (Figures S3A and S3B) with increased polyubiquitination (Figures S3C and S3D).

Reduction of NMDAR-Dependent Synaptic Responses in Cortexes of Shank3(+/ΔC) Mice, without Changes in Synapse Number or Morphology

As NR1 is an obligatory subunit of functional NMDAR, we predicted that a change in NR1 levels would alter NMDAR-dependent synaptic responses. Using acute cortical slices from frontal cortexes of 3- to 4-week-old mice, we monitored the amplitude of evoked responses in layer 2/3 cortical neurons following stimulation of presynaptic fibers in layer 4, using conditions that separately reveal AMPA- and NMDAR-dependent responses. The ratio of the NMDA/AMPA-dependent responses in Shank3(+/ΔC) cortex was reduced compared to the WT mice (0.38 ± 0.07 in the Shank3(+/ΔC); 0.70 ± 0.06 in littermate WT; $p < 0.005$) (Figure 4A, Figures S4A and S4B). The voltage dependence of the evoked AMPA current was similarly linear in WT and Shank3(+/ΔC) (Figure S5A). The AMPAR-mediated miniature excitatory postsynaptic current (EPSC) amplitude and frequency were unaltered (WT 15.2 ± 1.2 pA, 10.3 ± 1.7 Hz; Shank3(+/ΔC) 15.4 ± 0.9 pA, 8.6 ± 0.9 Hz) (Figure 4B and Table S1). These results are consistent with biochemical data and suggest a selective reduction of synaptic NMDAR responses.

Shank3 has been postulated to be a scaffolding molecule with putative roles in PSD maintenance, spine morphogenesis, and NMDAR and AMPAR function (Roussignol et al., 2005). Accordingly, we assessed whether changes in synaptic function might be coupled to cyto-architectural changes. We prepared electron

(D) Representative confocal images from DIV 14–21 cortical cultures colabeled with Shank3 (JH3025), Psd-95, and Vglut1. Cortical cultures from ΔC/ΔC mice were used as control for Shank3 Ab. Scale bar, 10 μm.

(E) Quantification of puncta density (see Experimental Procedures) from (D). 7000–11,000 μm of dendrites was examined from culture sets from three independent littermate pairs; **$p < 0.01$.

(F) Quantification of synaptic protein per μm from (D). Synaptic protein was defined as an area overlap between Shank3 or Psd-95 and the synaptic marker Vglut1. 7000–9000 μm of dendrites was examined from culture sets from three independent littermate pairs; **$p < 0.01$.

(G) Quantification of brain Shank3 mRNA levels from real-time PCR analysis. n = 3 independent littermate pairs; difference nonsignificant.

All quantitative data are shown as means ± SEM. All p values are derived from a Student's t test. See also Figure S1.

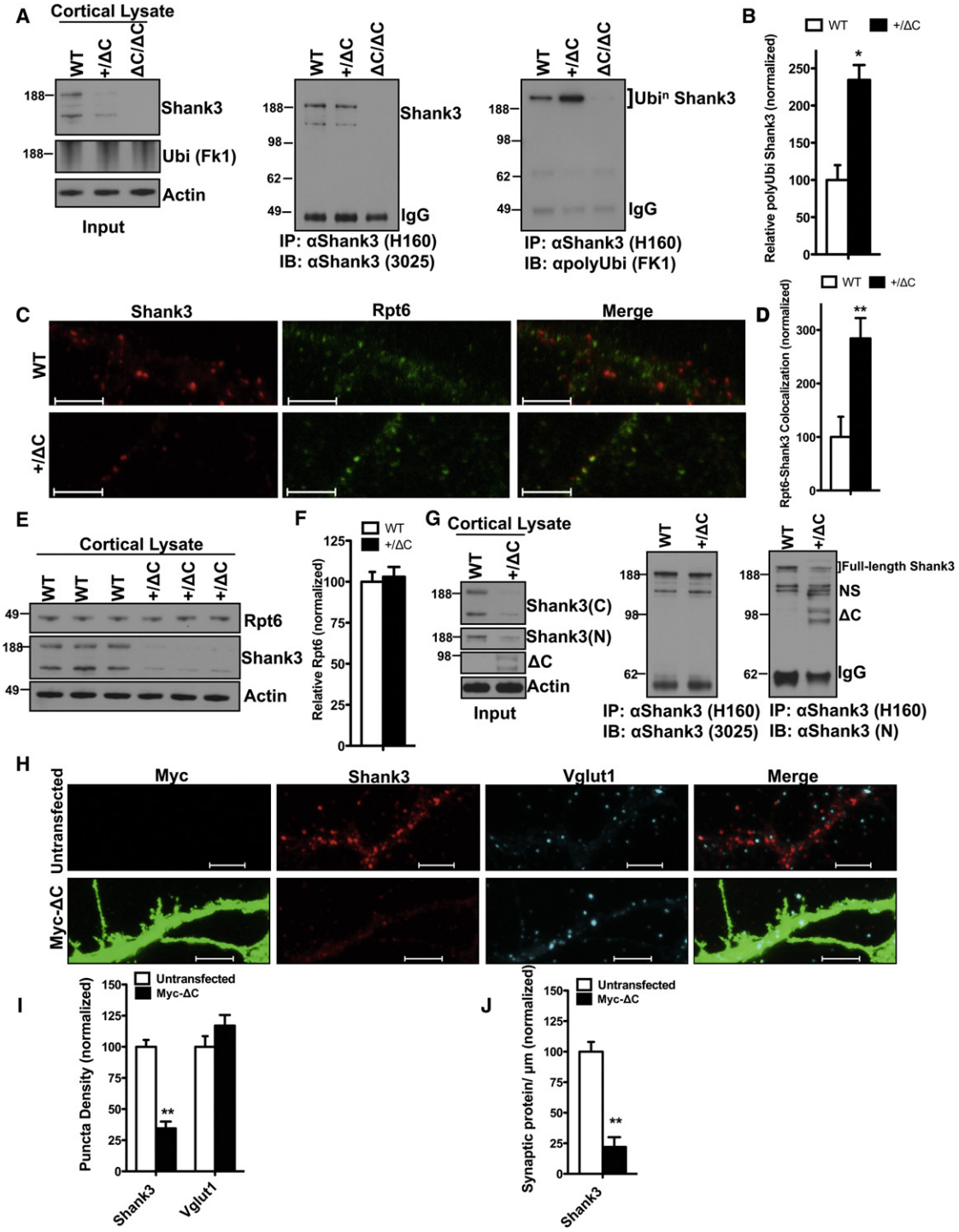

Figure 2. Increased Polyubiquitination of Shank3 Is Mediated by ΔC

(A) Coimmunoprecipitation assay from cortical lysates to assess in vivo polyubiquitination of Shank3 in the +/ΔC mouse. Polyubiquitinated Shank3 ran at ~250 kDa because of added polyubiquitin. Lysates from Shank3(ΔC/ΔC) were used as negative control.

(B) Quantification of relative Shank3 polyubiquitination from (A) (normalized to WT). y axis is FK1 polyubiquitin signal relative to immunoprecipitated Shank3. n = 3 independent littermate pairs; *p < 0.05.

(C) Representative confocal images from DIV 14–21 cortical cultures from WT and Shank3(+/ΔC) colabeled with Shank3 and the proteasomal marker Rpt6. Scale bar, 5 μm.

(D) Quantification of colocalization (area overlap per μm of dendrite) between Shank3 and Rpt6 from (C). 5000–7000 μm of dendrites was examined from culture sets from three independent littermate pairs; **p < 0.01.

microscopy (EM) images of layer 5 somatosensory cortexes of 8-week-old mice and found no change in PSD length or thickness in Shank3(+/ΔC) mice (Figures 4C–4E). We also examined spine density by labeling neurons in fixed tissue with biolistic-DiI (Figure 4F) and performed automated counting and found no change in spine density (Figure 4G) or spine volume (Figures 4H–4J and Figure S4D) in 8-week-old Shank3(+/ΔC) mice. Similarly, synapsin staining of DIV 14–21 cortical neurons revealed identical puncta density in Shank3(+/ΔC) and WT mice (Figures S5B and S5C). These data indicate that spine and synapse formation are not altered in representative regions of adolescent Shank3(+/ΔC) brain and cultured neurons and are consistent with preservation of spontaneous miniature excitatory postsynaptic current (mEPSC) frequency and amplitude in Shank3(+/ΔC) brain. Accordingly, changes in NMDAR function are likely due to reduced expression rather than spine dysmorphogenesis or deficits of synapse formation.

NMDAR and Group I mGluR Synaptic Plasticity Are Altered in Hippocampi of Shank3(+/ΔC) Mice

We used acute hippocampal slices to assess whether NR1 reduction in the Shank3(+/ΔC) mice alters aspects of synaptic plasticity. We first examined the efficacy of Schaffer collateral-CA1 synapses by monitoring the evoked field excitatory postsynaptic potential (fEPSP) following paired pulses as an indicator of presynaptic function. This response was not different between WT and Shank3(+/ΔC) mice (Figure S5D). Similarly, analysis of the amplitude of the presynaptic fiber volley relative to both the initial slope of the fEPSP (Figure S5E) and the peak of the population spike (Figure S5F) revealed no change in either relationship. The former indicates that basal synaptic efficacy was unaltered, and the combination of both measures suggests that the intrinsic conductances underlying spike generation are not altered in Shank3(+/ΔC) mice.

LTP was induced by four trains of high-frequency stimulation with an inter-train interval of 5 min. In WT, fEPSP increased to 170.8% ± 8.3% of baseline immediately after stimulation (t = 60 min) and sustained at the level of 158.4% ± 13.8% of baseline at t = 180 min (Figure 5A). In Shank3(+/ΔC) mice the magnitude of LTP induction was significantly reduced (143.1% ± 5.6% of baseline at t = 60 min after stimulation) and decayed more rapidly than in WT mice (115.1% ± 4.9% of baseline at t = 180 min, $p < 0.005$, Student's t test). NMDAR-dependent LTD of Schaffer collateral-CA1 synapses was also reduced in Shank3(+/ΔC) mice. LTD was evoked using low-frequency synaptic stimulation (LFS) and resulted in a stable reduction of synaptic strength to 82.0% ± 3.3% of baseline at t = 30 min (Figure 5B). In Shank3(+/ΔC) mice, the initial synaptic depression was not different from WT but beginning after 20 min returned to near prestimulus baseline (95.7% ± 2.9% of baseline at t = 30 min, $p < 0.05$, Student's t test). These findings are consistent with a reduction of postsynaptic NMDAR function.

Next we examined mGluR-dependent chemical LTD in slices from 3- to 4-week-old Shank3(+/ΔC) mice. LTD of Schaffer collateral-CA1 synapses was induced by the group I mGluR agonist DHPG (100 μM) for 5 min. In WT slices, bath-applied DHPG resulted in a stable reduction of synaptic strength (69.1% ± 5.0% of baseline at t = 90 min) (Figure 5C). In Shank3(+/ΔC) mice, mGluR-LTD by DHPG was increased (56.9% ± 3.8% of baseline at t = 90 min, $p < 0.05$, Student's t test). Similarly, LTD produced by paired-pulse low-frequency stimulation (PP-LFS: 1 Hz for 20 min) was increased in the Shank3(+/ΔC) mice (88.7% ± 1.9% of baseline at t = 40 min in WT mice compared to 74.3% ± 4.6% of the baseline at t = 40 min in Shank3(+/ΔC) mice) (Figure 5D). The increase of mGluR-LTD in the Shank3(+/ΔC) is similar to the increase in *Fmr1* KO mice. However, unlike the fragile X model, the mGluR-LTD increase in the Shank3(+/ΔC) mice was completely inhibited by the protein synthesis inhibitor cycloheximide (Figure 5E), indicating that the mechanism affecting mGluR-LTD may be different in these two models.

Shank3(+/ΔC) Mice Display Selective Deficits of Social Interactions

We first examined cognitive function, as a baseline for studies of social interactions. Long-term spatial memory tested in a classic version of the Morris water maze (Figures S6A and S6B) as well as short-term spatial recognition and spatial working memory (Table S2) were not different between Shank3(+/ΔC) and WT mice. In addition, a classical fear-conditioning paradigm showed that context and cue-related fear memory and extinction in Shank3(+/ΔC) mice were similar to WT (Figures S6C and S6D). Shank3(+/ΔC) mice also showed normal anxiety levels (Table S2) and learning of motor skills (Figure S6E). These data indicate that Shank3(+/ΔC) mice exhibit preserved learning and memory functions.

A separate group of Shank3(+/ΔC) mice was tested in a set of social tasks in which accessibility and familiarity of social stimuli were modulated in a controlled fashion. First, we analyzed reciprocal social interactions in a habituation-dishabituation paradigm that provides a measure of hippocampus- and amygdala-dependent social memory and has been used in mouse models associated with ASD (Ferguson et al., 2002). As expected, WT mice showed a decrease in duration of social investigation during repeated presentations of the same stimulus mouse followed by a reactivation of investigation when a novel

(E) Representative Immunoblot from total cortical lysates showing total Rpt6 levels in WT and Shank3(+/ΔC) mice.
(F) Quantification of protein levels in (E). n = 3 independent littermate pairs; $p > 0.05$.
(G) Coimmunoprecipitation assay from cortical lysates showing that ΔC binds full-length Shank3 in vivo. The input lysates were blotted with JH3025 Shank3 (C) and the N-terminal Shank3 Ab (N). Protein samples in the input were immunoprecipitated with Shank3 (H-160) Ab and analyzed for ΔC binding using the N-terminal Shank3 Ab that recognized the ΔC band in the +/ΔC but not the WT lane. NS = nonspecific bands.
(H) Representative confocal images from DIV 12–14 WT cortical cultures 24 hr after Myc-ΔC transient transfection. Scale bar, 5 μm.
(I) Quantification of puncta density from (H). 5000–7000 μm of dendrites was examined from three independent culture sets; $^{**}p < 0.01$.
(J) Quantification of synaptic protein per μm from (H). Synaptic protein was defined as an area overlap between Shank3 and Vglut1. 5000–7000 μm of dendrites was examined from three independent culture sets; $^{**}p < 0.01$.
All quantitative data are shown as means ± SEM. All p values are derived from a Student's t test. See also Figure S2.

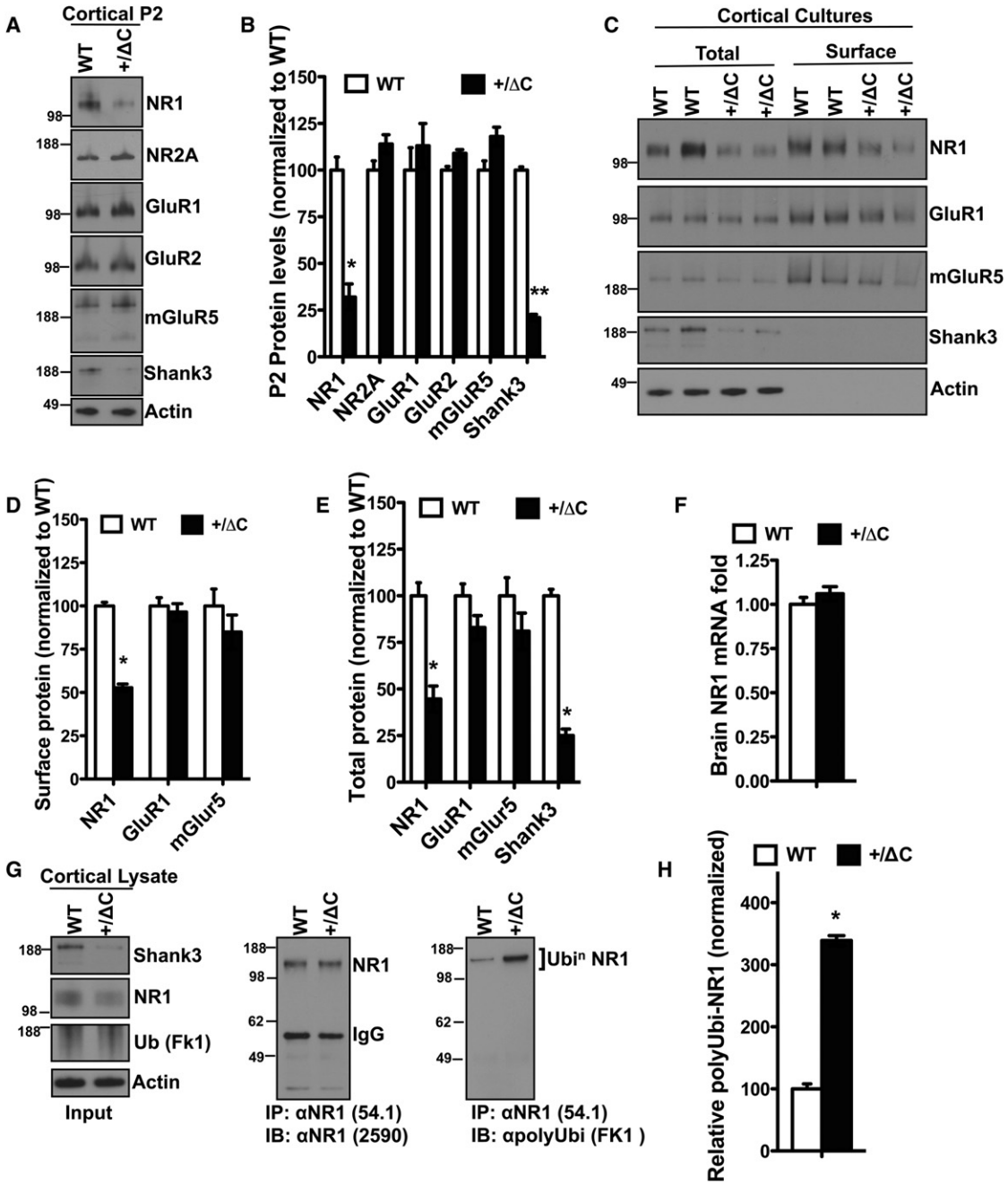

Figure 3. NR1 Reduction in the Shank3(+/ΔC) Mice Is due to Enhanced Polyubiquitination

(A) Representative immunoblots from cortical P2 (synaptoneurosomal) fractions from WT and Shank3(+/ΔC) mice aged P42.

(B) Quantification of protein levels in (A). n = 3 independent littermate pairs; $^{**}p < 0.01$; $^{*}p < 0.05$.

(C) Representative immunoblots from DIV 14–21 cortical cultures from two independent WT and Shank3(+/ΔC) sets. Surface samples are from biotinylated lysates immunoprecipitated with avidin.

(D) Quantification of surface protein levels in (C). n = cultures from three independent littermate pairs; $^{*}p < 0.05$.

(E) Quantification of total protein levels in (C). n = cultures from three independent littermate pairs; $^{*}p < 0.05$.

(F) Quantification of brain NR1 mRNA levels from real-time PCR analysis. n = 3 littermate pairs; difference is nonsignificant.

(G) Coimmunoprecipitation assay from cortical lysates to assess in vivo polyubiquitination of NR1 in the Shank3(+/ΔC) mice.

(H) Quantification of in vivo NR1 polyubiquitination from (G). y axis is FK1 polyubiquitin signal relative to immunoprecipitated NR1. n = 3 independent littermate pairs; $^{*}p < 0.05$.

All quantitative data are shown as means ± SEM. All p values are derived from a Student's t test. See also Figure S3.

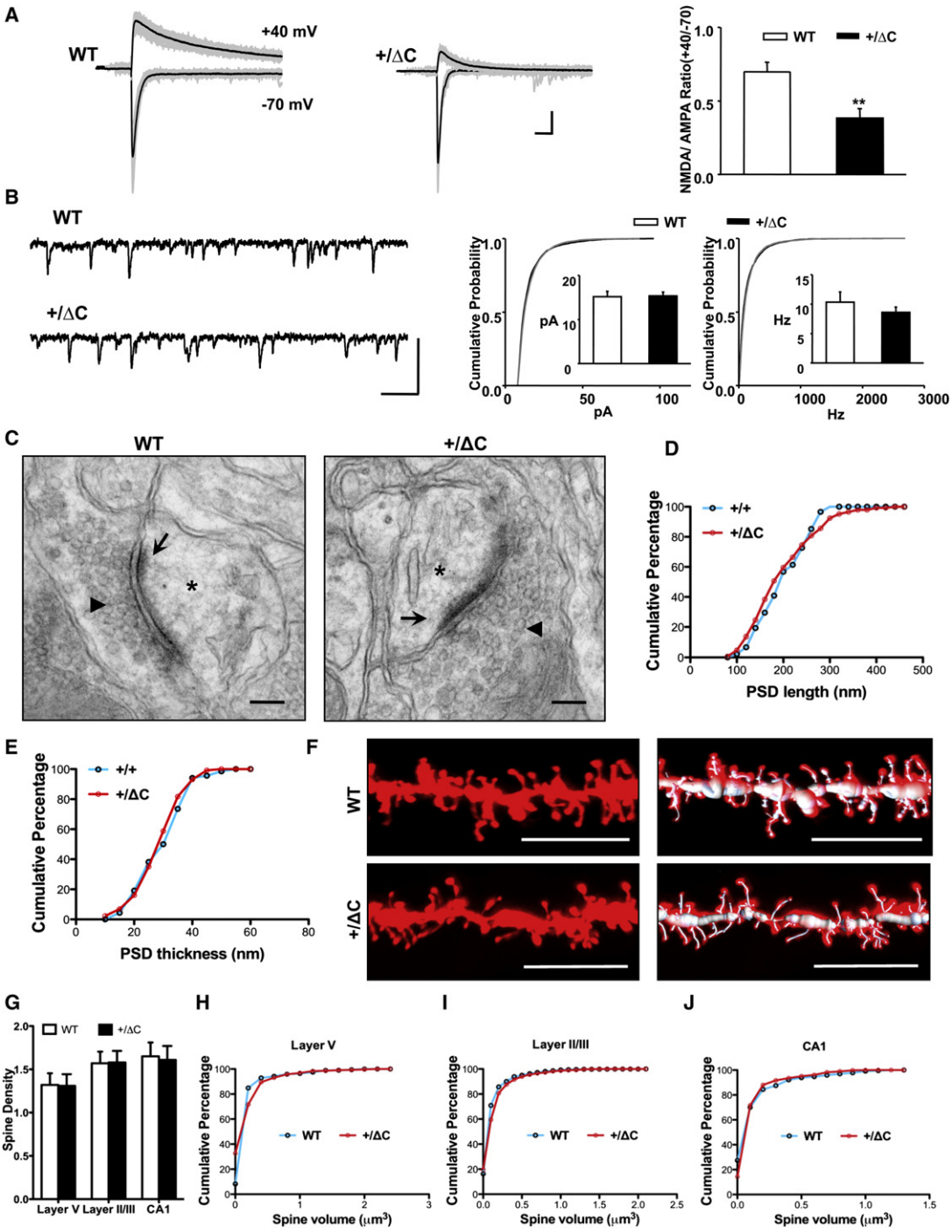

Figure 4. Reduction of NMDAR-Mediated Synaptic Responses in Cortexes of Shank3(+/ΔC) Mice, without Changes in Spine Number or Morphology

(A) Raw (gray) and averaged (black) traces from a series of 20 consecutive evoked EPSCs in cortical slices. The NMDA/AMPA ratio is diminished in Shank3(+/ΔC) neurons (n = 15, 5 mice) compared with WT (n = 9, 4 mice). **p < 0.005 (scale bars, 50 pA/50 ms).

(B) Representative whole-cell recording traces and cumulative probability (CP) distribution of AMPA mEPSC amplitude and frequency from all events in WT (n = 22) and Shank3(+/ΔC) (n = 23) neurons. Differences are nonsignificant for both amplitude and frequency. Inset: bar graphs represent the mean amplitude or frequency of each population ± SEM (scale bars, 50 pA/0.1 s).

(C) Exemplar electron micrographs of spine synapses in layer V of the somatosensory cortexes from WT and Shank3(+/ΔC) mice showing the presence of the postsynaptic density (arrows), synaptic vesicles (arrowheads), and dendritic spines (asterisks). The following quantifications in (D) and (E) are from spine synapses in layer V of the somatosensory cortex. scale bar = 100 nm.

stimulus mouse was presented (Figure 6A). Approximately half of the WT mice showed a short single bout of aggression per trial (Figure 6D, Figures S6F and S6I). The presence of these aggression episodes did not disrupt normal habituation-dishabituation curves in WT mice (Figures 6B and 6C). By contrast, Shank3(+/ΔC) mice displayed significantly lower levels of social investigation (Figure 6A) that were modulated by the presence of aggressive episodes (Figures 6B and 6C). Shank3(+/ΔC) mice with aggressive behaviors showed significantly less social investigation as compared to WT (Figure 6C), whereas Shank3(+/ΔC) mice that did not demonstrate aggression were not different from controls (Figure 6B).

A similar interference between aggressive behaviors and social investigation was observed in a separate cohort of Shank3(+/ΔC) mice exposed to stimulus mice of different strain backgrounds (Figures S6G and S6I). Multiple tests for odor recognition and discrimination (Figures S6K and S6L) indicated preserved olfactory processing in Shank3(+/ΔC) mice. A sharp increase in aggression toward a novel stimulus mouse observed in Shank3(+/ΔC) mice (Figure 6D, Figure S6F) suggested preserved social recognition memory as well. This was confirmed by additional testing in a situation where aggression toward a stimulus mouse is prevented by placing the stimulus mouse under an enclosure. In this situation, Shank3(+/ΔC) mice showed levels of social investigation comparable to those in WT (Figure 6E). These data indicate that Shank3(+/ΔC) mice have preserved social recognition memory but display aberrant social interactions with aggressive behaviors.

To test whether Shank3(+/ΔC) mice are more aggressive in general, we employed two commonly used protocols: neutral arena and resident-intruder tests. As expected, aggressive behaviors significantly intensified when tested in the resident-intruder test (Figure 6F, Figure S4J); however there were no genotype-related differences in any of the test conditions. These data indicate that increased aggressive behaviors observed in Shank3(+/ΔC) mice during the dishabituation stage of the social recognition task were not a result of general augmentation of aggression.

To analyze possible changes in social motivation of Shank3(+/ΔC) mice, we tested approach behaviors to enclosed male or female conspecifics. Shank3(+/ΔC) mice spent more time investigating an enclosed male stimulus mouse than WT mice (Figures 6G and 6I). This difference remained significant after repeated testing (Figure 6J), indicating that the increase in social investigation of an enclosed male mouse was not a result of generalized exploratory activation of Shank3(+/ΔC) mice. The same mice were then tested with a sexually receptive enclosed female. Total duration of social investigation was similar between Shank3(+/ΔC) and WT mice (Figures 6H and 6K), but measures that specifically reflect an approach behavior showed significant genotype-related differences. The approach latency in Shank3(+/ΔC) was significantly longer than WT (Figure 6L). To confirm this finding, an additional cohort of sexually naive male mice was tested during reciprocal interactions with females. Because in this situation the approach behavior can be affected by a free-roaming female mouse, we recorded ultrasonic calls that males emit in the presence of females. Latencies to the first ultrasound call emitted by Shank3(+/ΔC) mice were significantly longer than WT (Figure 6M). Thus, these data indicate that Shank3(+/ΔC) mice have significant differences from WT in social approach behavior, communications, and social reciprocal interactions with male and/or female conspecifics.

Shank3(+/ΔC) Mice Display Behavioral Traits Consistent with Reduced NMDAR Function

Schizophrenia-related phenotypes are reported in mouse models with reduced NMDAR function (Mohn et al., 1999). Accordingly, we extended our battery of behavioral tasks to include schizophrenia-related phenotypes in Shank3(+/ΔC) mice. We first utilized prepulse inhibition of startle reaction (PPI). In this paradigm, a brief, low-intensity acoustic stimulus (the prepulse) inhibits the startle reflex caused by a loud stimulus. Shank3(+/ΔC) mice showed significantly lower amplitudes and longer latencies of startle response than WT (Figure 7A; Figures S7A–S7D). The levels of prepulse inhibition were not different between genotypes as assessed by ANOVA (Figure 7B). However, the prepulse inhibition in WT was negatively correlated with startle amplitude (Figures 7C–7D; Figure S5E; Tables S3) resulting in an underestimation of prepulse inhibition in the control group due to their higher levels of startle (Figure 7A). To correct for these differences we employed an analysis of covariance (ANCOVA) with the amplitude of startle reaction as a continuous predictor variable. This analysis revealed a significant effect of Genotype and Genotype × Trial interaction due to differences between Shank3(+/ΔC) and WT in the most challenging type of trials, which consisted of a combination of the highest level of startle stimulus and the lowest level of prepulse (Figure 7E).

We also tested sensitivity to psychostimulants; a preclinical correlate of positive symptoms used extensively in animal models of schizophrenia (Powell and Miyakawa, 2006). Systemic injection of dizocilpine (MK-801), a noncompetitive NMDAR

(D) The PSD length is not significantly different in the WT and the +/ΔC mice. n = 88 for WT; n = 146 for Shank3(+/ΔC); $p > 0.05$.
(E) The PSD thickness is not significantly different in the WT and the +/ΔC mice. n = 68 for WT; n = 131 for Shank3(+/ΔC); $p > 0.05$.
(F) Representative DiI-labeled images of layer V pyramidal neurons of the somatosensory cortexes from WT and Shank3(+/ΔC) mice. To the right are 3D reconstructions depicting faithful labeling of spines by the filament module in Imaris. Scale bar, 10 μm.
(G) Quantification of spine density (spines per μm) in layer V, layer II/III pyramidal neurons of the somatosensory cortex, and CA1 pyramidal neurons from WT and Shank3(+/ΔC) mice. n = 9–29 cells from three independent littermate pairs. Difference is nonsignificant.
(H) Quantification of spine volume in layer V pyramidal neurons of the somatosensory cortexes from WT and Shank3(+/ΔC) mice. n = 671 spines from three independent littermate pairs. $p > 0.05$.
(I) Quantification of spine volume in layer II/III pyramidal neurons of the somatosensory cortexes from WT and Shank3(+/ΔC) mice. n = 2805 spines from three independent littermate pairs. $p > 0.05$.
(J) Quantification of spine volume in CA1 pyramidal neurons from WT and Shank3(+/ΔC) mice. n = 853 spines from three independent littermate pairs. $p > 0.05$.
All quantitative data are shown as means ± SEM. All p values are derived from a Student's t test. See also Figure S4.

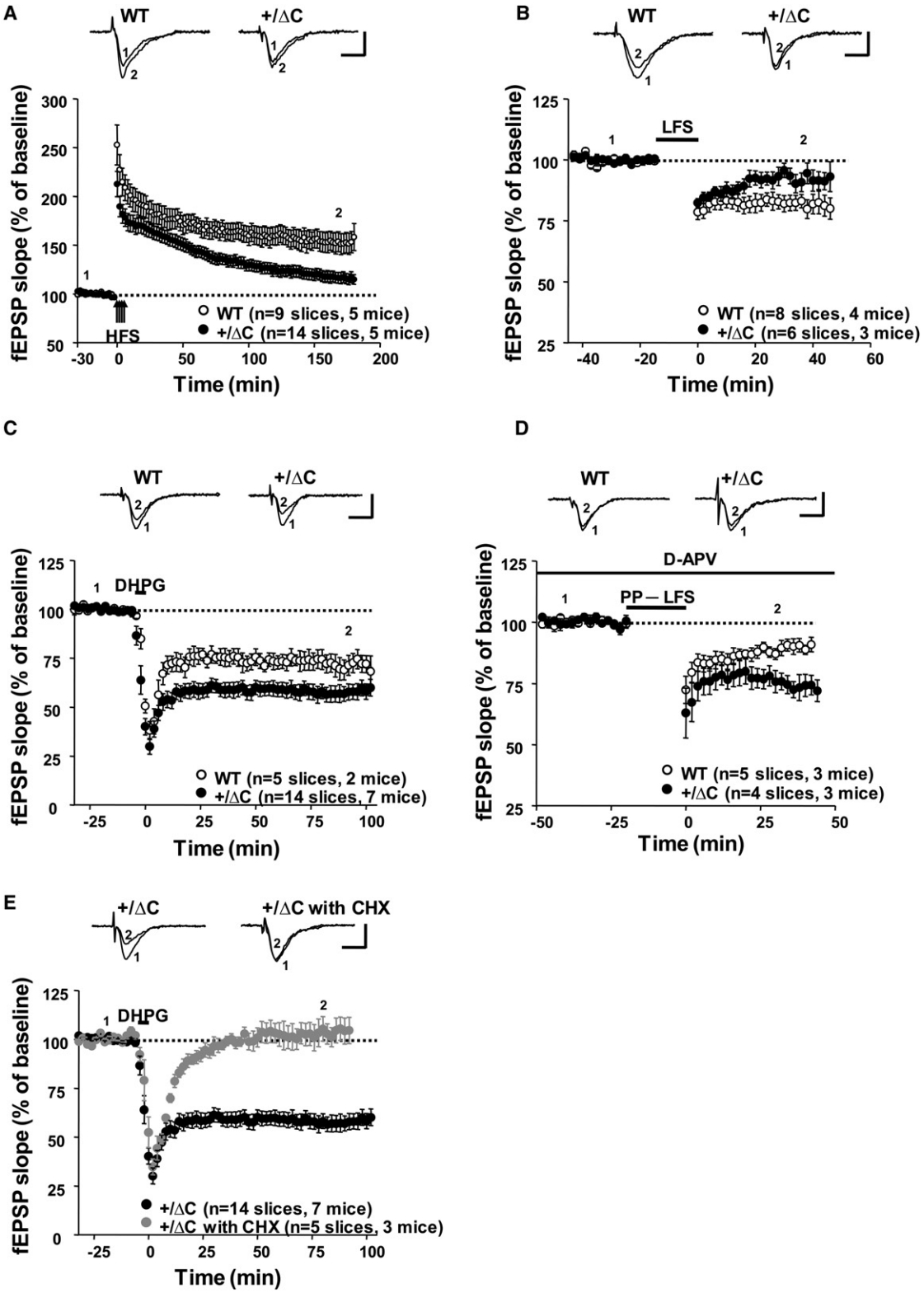

Figure 5. NMDAR-Dependent LTP and LTD and Group I mGluR-LTD Are Altered in Hippocampal Slices Derived from Shank3(+/ΔC) Mice

(A) HFS-induced LTP is significantly more reduced in Shank3(+/ΔC) mice than in littermate WT. $p < 0.005$ (scale bars, 1 mV/10 ms).

(B) NMDAR-dependent LTD of Schaffer collateral-CA1 synapses is reduced in Shank3(+/ΔC) mice. $p < 0.05$ (scale bars, 1 mV/10 ms).

antagonist, dose-dependently increased locomotor activity in both genotypes (Figure 7F) However, the levels of motor activation were significantly higher in Shank3(+/ΔC) compared to WT (Figure 7G). Similarly, amphetamine, a known psychostimulant that exerts its action through release of dopamine, resulted in a significantly stronger activation in Shank3(+/ΔC) compared to WT (Figures 7H and 7I). By contrast, Shank(+/ΔC) mice did not show novelty-induced hyperactivity (Figures S7J and S7H), indicating that the increased motor activity induced by MK-801 and amphetamine is specific to these agents.

DISCUSSION

The present study supports a ''gain-of-function'' mechanism for synaptic and behavioral dysfunction in a mouse model designed to mimic human mutations of Shank3 associated with ASD (Durand et al., 2007). In combination with observations from Homer KO mice, we propose a model in which perturbations that reduce the stability of the Homer-Shank3 protein complex result in increased ubiquitination of Shank3 and reduced expression at the synapse. Changes of NR1 expression and ubiquitination are coupled to changes in Shank3. Determinants of the stability of the Homer-Shank protein complex have been reported in biochemical and crystallographic studies (Hayashi et al., 2009) and are consistent with our findings. Our model is also consistent with a report that Shank proteins undergo ubiquitination in physiological adaptations to neuronal activity (Ehlers, 2003). Data regarding effects of reduced expression of Homer crosslinking proteins include reduced Shank3 and NR1 expression and increased ubiquitination in Homer triple KO, Homer1 KO, and Homer2/3 KO brain. Moreover, Homer1a expression, which inhibits the formation of Homer-Shank3 complex (Hayashi et al., 2009), mimics Homer KO to reduce Shank3 expression, whereas selective genetic deletion of Homer1a results in increased Shank3 and reduced ubiquitination in brain. In extending this model to include the effect of Shank3 mutation, we note that Shank3ΔC protein is stably expressed in the Shank3(+/ΔC) mice and physically associates with full-length Shank3 from brain. Because Shank3ΔC lacks the Homer-binding domain and associates with full-length Shank3, its incorporation with WT Shank3 effectively reduces Homer crosslinking of the Homer-Shank3 protein complex. Acute overexpression of Shank3ΔC in neurons reduces WT Shank3, providing evidence that downregulation of WT Shank3 is due to Shank3ΔC expression. We do not detect ubiquitination of Shank3ΔC even from Shank3(ΔC/ΔC) brain, which mitigates the notion that Shank3ΔC is primarily ubiquitinated and ''drags'' the rest of the proteins along. This model predicts that any mutation of Shank3 or Homer that effectively reduces the stability of the Homer-Shank complex will lead to increased ubiquitination and proteasomal degradation of Shank3 and NR1. This could include deletions or point mutations of Shank3 that limit their physical assembly with other Shank3 molecules or Homer. Consistent with this model, Homer1 KO mice exhibit behavioral phenotypes (Szumlinski et al., 2005) similar to those of Shank3(+/ΔC) mice.

Our model begs the question of why Shank3 expression and ubiquitination should be sensitive to physical association with Homer. We note that manipulations of Homer1a can influence Shank3 expression and ubiquitination, and this reinforces the notion that Shank3 is a nodal point for regulation of synaptic function in response to natural activity. Homer1a expression is tightly linked to behavioral experience (Brakeman et al., 1997) and can also be induced by a variety of pharmacological and pathological stimuli. Thus, dynamic expression of Homer1a could contribute to the disassembly of Homer-Shank3 complexes, especially if the complex is weakened by mutations of Shank or Homer. By this mechanism, Homer1a expression could contribute to the pathogenesis of ASD.

Our studies also suggest a link between Shank3 and group I mGluR function. The molecular basis of enhanced mGluR-LTD in Shank3(+/ΔC) does not appear to be linked to altered expression of mGluRs. mGluR-LTD is increased in Fmr1 KO mice and this has been linked to neurological deficits in this mouse and in patients with fragile X disease (Bear et al., 2004). Thus, enhanced mGluR-LTD may contribute to behavioral deficits in the Shank3(+/ΔC) mice.

Shank3(+/ΔC) mice exhibit behavioral phenotypes that parallel symptoms of ASD. The most striking differences between Shank3(+/ΔC) and WT mice were observed in a social recognition test that allowed for engagement in reciprocal interactions. Shank3(+/ΔC) mice reacted to novel conspecifics by a sharp increase in aggression rather than an increase in social investigation. Aggressive behaviors of Shank3(+/ΔC) mice were not generalized across different tasks, indicating that the exaggerated aggression is likely a reaction to changes in social routine rather than a result of their generalized aggressiveness. Inferences regarding phenotypic relevance between mouse and human behaviors, such as aggression in individuals with ASD (Kanne and Mazurek, 2010), are difficult; however, the findings of exaggerated aggressiveness to novel conspecifics as well as deficits in ultrasound vocalization and alterations in social approach behaviors indicate that the effects of Shank3(+/ΔC) mutation are detected on multiple domains of social interactions tested in a species-specific manner.

The decrease in NR1 observed in Shank3(+/ΔC) mice invites comparisons with mice hypomorphic for NR1 (Mohn et al., 1999). The preserved structure of synapses and spines that are observed in Shank3(+/ΔC) mice is consistent with reports from the conditional NR1 KO where NR1 excision within CA1 did not affect spine density (Rampon et al., 2000). The most striking difference between mice hypomorphic for NR1 and Shank3(+/ΔC) mice is that behavioral phenotypes of Shank3(+/ΔC) mice occur in the context of normal cognitive

(C) mGluR-dependent chemical LTD induced by DHPG is enhanced in Shank3(+/ΔC) mice. $p < 0.05$ (scale bars, 1 mV/10 ms).
(D) LTD produced by paired-pulse low-frequency stimulation is increased in the Shank3(+/ΔC) mice. The mean values were significantly different 30 min after stimulation. $p < 0.05$ (scale bars, 1 mV/10 ms).
(E) mGluR-LTD expressed in Shank3(+/ΔC) mice is completely blocked by protein synthesis inhibitor cycloheximide (CHX, 60 μM). Scale bars, 1 mV/10 ms.
All quantitative data are shown as means ± SEM. All p values are derived from a Student's t test. See also Figure S5.

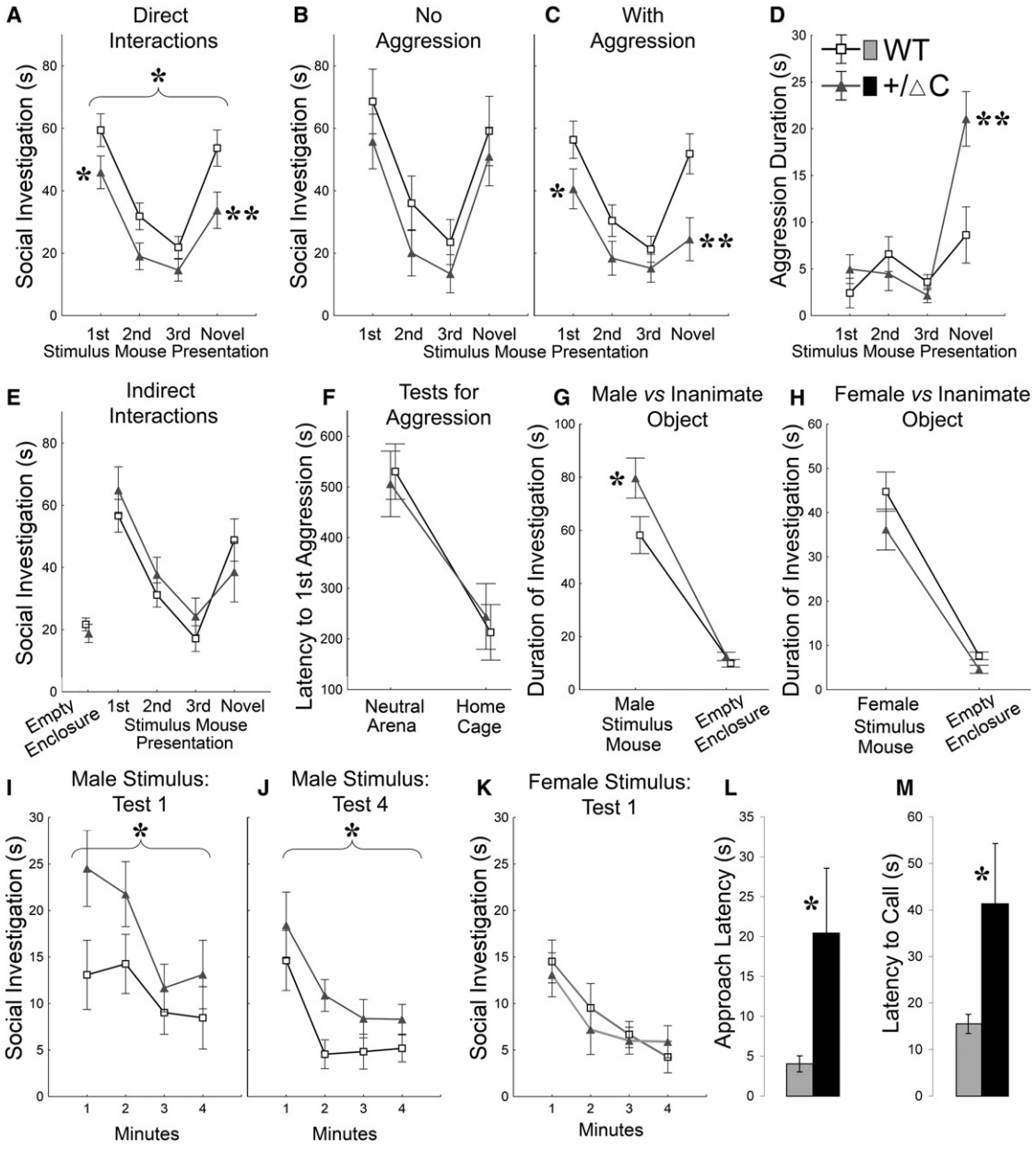

Figure 6. Shank3(+/ΔC) Mice Display Aberrant Social Behaviors in Reciprocal and Indirect Social Interactions

(A) Duration of social investigation of a free-roaming stimulus mouse in consecutive trials of the habituation-dishabituation paradigm. Brackets indicate a significant main effect of genotype ($p < 0.05$); asterisks show between-genotype differences at a particular trial (*$p < 0.05$ and **$p < 0.01$) (n = 20 per genotype).

(B) Social investigation as in (A) for subgroups of Shank3(+/ΔC) (n = 9) and WT (n = 8) that showed no aggressive behaviors during testing. Difference nonsignificant.

(C) Social investigation as in (A) for subgroups of Shank3(+/ΔC) (n = 11) and WT (n = 12) that showed aggressive behaviors during testing.

(D) Duration of aggressive behaviors for the groups of mice shown in (C).

(E) Social investigation of an enclosed stimulus mouse in consecutive trials of the habituation-dishabituation paradigm. No significant differences were found between Shank3(+/ΔC) (n = 12) and WT (n = 14). The same test mice were used for (E)–(L).

(F) Latency to the first aggression episode in a neutral arena and in a test mouse's home cage.

(G and H) Duration of investigation of an enclosed male (G) or female (H) mouse and an inanimate empty enclosure.

(I and J) Dynamics of social investigation of an enclosed male stimulus mouse in novel (I) and familiar environment (J). The 1st (I) and the 4th (J) repetitions of the test are shown.

(K) Dynamics of social investigation of an enclosed female stimulus mouse in familiar environment. The test was conducted in the same environment as (I)–(J). No between-genotype differences were observed.

(L) Latency of the first approach to an enclosed female measured during the test shown in (H) and (K). Shank3(+/ΔC) mice (n = 12) took significantly longer to approach the social stimulus than WT (n = 14) (Student's t test, $p < 0.05$).

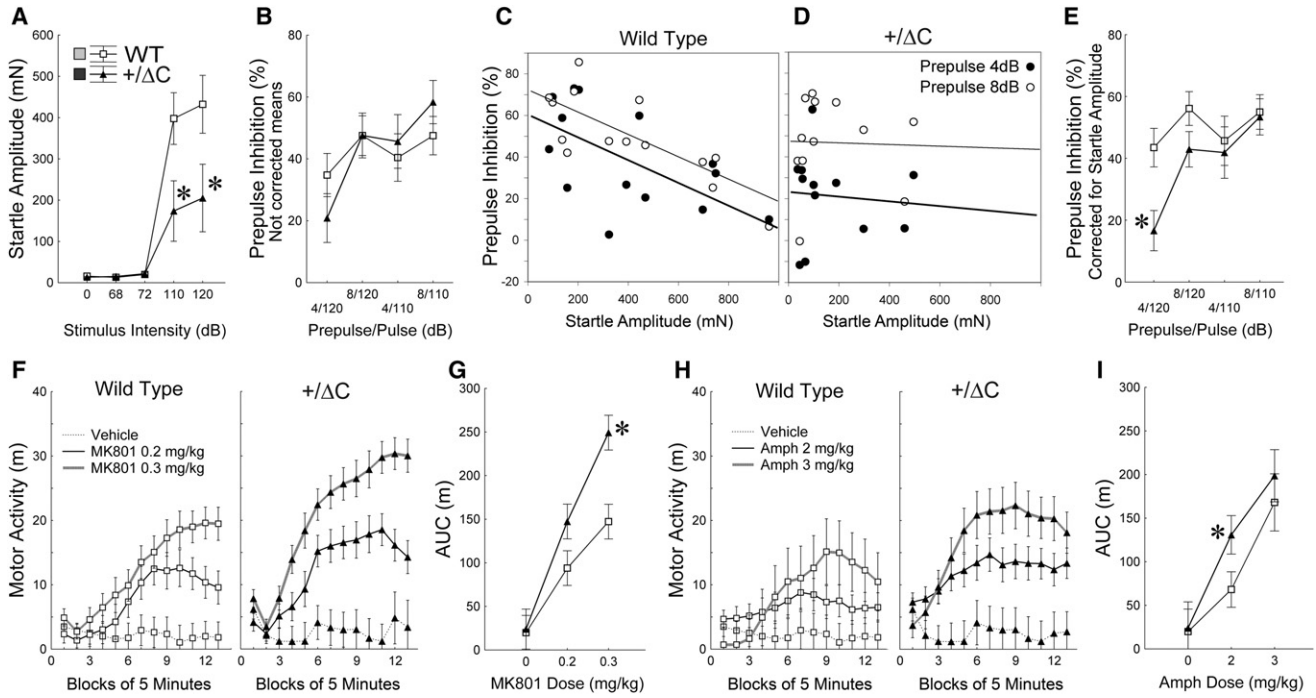

Figure 7. Shank3(+/ΔC) Mice Display Schizophrenia-Related Behavioral Phenotypes but Preserved Spatial and Fear Memories

(A) Amplitude of acoustic startle reaction as a function of stimulus intensity. Asterisks indicate that amplitudes of reactions to startle stimuli (110 or 120 dB) in Shank3(+/ΔC) mice (n = 12) were significantly lower than in WT (n = 14) ($p < 0.001$). The stimuli used as prepulses (68 and 72 dB) did not evoke startle reactivity in either of the genotypes.

(B) Raw means of prepulse inhibition uncorrected for differences in startle reactivity between Shank3(+/ΔC) and WT.

(C and (D) Scatterplots of the startle amplitude (x axis) and levels of prepulse inhibition (y axis) in trials with a 120 dB startle stimulus for WT (C) and Shank3(+/ΔC) (D) mice. Thick and thin lines show linear regression lines fitted to the data from the trials with 4 or 8 dB prepulse, respectively. Pearson correlations between these variables were significant for WT but not Shank3(+/ΔC) mice (see Table S3).

(E) Means of prepulse inhibition in WT and Shank3(+/ΔC) mice corrected by ANCOVA for significantly different levels of startle amplitude. Asterisk shows a significant between-genotype difference ($p < 0.01$).

(F and G) Motor activation (F) and dose-response (G) to MK-801. Area under the curve (G) was calculated from (F) as a total motor activity 15 min after an injection. Asterisks show a significant between-genotype difference ($p < 0.001$). WT n = 8,8,8 and Shank3+/ΔC n = 6,8,8 for MK-801 doses 0, 0.2, and 0.3 mg/kg, respectively.

(H and I) Motor activation (H) and dose-response (I) to amphetamine. Asterisk indicates a significant between-genotype difference ($p < 0.05$). WT n = 8,13,5 and Shank3(+/ΔC) n = 6,11,6 for amphetamine doses 0, 2, and 3 mg/kg, respectively.

Error bars in (A)– (I) are means ± SEM. See also Figure S7 and Table S3.

function as assayed in multiple tests of learning and memory. NMDAR-dependent LTP and LTD are reduced in Shank3(+/ΔC) hippocampus but are not absent, and plasticity is apparently sufficient for normal cognitive function. The preserved cognition in these mice mitigates the concern that aberrant social behaviors might arise nonspecifically in a mouse with major cognitive dysfunction and suggests that Shank3ΔC models will be useful to explore the cellular and developmental determinants of social deficits associated with ASD and to relate these to a molecular model that includes enhanced ubiquitination of NR1. Our studies, however, should not be taken as direct evidence of a role of Shank3 in schizophrenia because human genetic evidence remains incomplete. Genetic studies report linkage of schizophrenia at the 22q11-13 locus, which includes *Shank3* (Condra et al., 2007; DeLisi et al., 2002), but the single reported association of Shank3 mutations with schizophrenia (Gauthier et al., 2010) is notable for inclusion of patients with early onset symptoms that may overlap with ASD (Rapoport et al., 2009). Nevertheless, our study supports the notion that patients with ASD or schizophrenia may share the molecular pathology of reduced NMDAR function.

EXPERIMENTAL PROCEDURES

Detailed experimental methods are provided in the Extended Experimental Procedures.

(M) Latencies to the first ultrasound call emitted by Shank3(+/ΔC) mice (n = 11) in the presence of a free-roaming female were significantly longer than in WT (n = 11) (Student's t test, $p < 0.05$).

Brackets in (A) and (I)–(J) indicate a significant main effect of genotype ($p < 0.05$), and asterisks in (A)–(M) show between-genotype differences at a particular trial (*$p < 0.05$ and **$p < 0.01$). Error bars in (A)– (M) are means ± SEM. See also Figure S6, Table S2, and the Extended Experimental Procedures.

Animals

Mice were generated on a mixed 129s6; C57BL6/J background and backcrossed to C57BL6/J background to at least the F5 generation. Littermate pairs of male mice (unless otherwise noted) 3 to 6 months of age were used in behavioral testing. All procedures involving animals were under the guidelines of JHU and UTSW Institutional Animal Care and Use Committee.

Behavioral Testing

Behaviors were recorded by computer-based tracking systems (HVS Image Analysis VP-200, HVS Image, Hampton, England; Any Maze 4.72, Stoelting Co, Wood Dale, IL; Noldus, Ethovision 2.3.19, SR-LAB, San-Diego Instruments, CA, USA) and scored when necessary by trained observers blind to genotype using a computer-assisted data acquisition system.

Measuring In Vivo Ubiquitination

The ubiquitination of Shank3 and NR1 was measured from cortical lysates and is described in detail in the Extended Experimental Procedures.

Electrophysiology

Electrophysiology was done using standard techniques. Details are provided in the Extended Experimental Procedures.

Statistical Analyses

The behavioral data were analyzed using ANOVA/ANCOVA with the statistical package STATISTICA 8.0 (StatSoft, Tulsa, OK, USA) and a minimal level of significance $p < 0.05$. Fisher LSD post-hoc tests were applied to significant main effects or interactions. All data are shown as means ± standard error of the mean (SEM) unless noted otherwise.

SUPPLEMENTAL INFORMATION

Supplemental Information includes Extended Experimental Procedures, seven figures, and three tables and can be found with this article online at doi:10.1016/j.cell.2011.03.052.

ACKNOWLEDGMENTS

M.A.B., A.S., B.X., and P.F.W. designed the study. M.A.B. executed and analyzed all the biochemistry, immunocytochemistry, and DiI experiments. B.X., M.A.B., D.W., Y.C., and X.Z. created the Shank3 mouse. J.M.P., S.K.J., and J.K. did the electrophysiology experiments and analysis supervised by P.F.W. and D.J.L. R.S.P. did the electron microscopy. T.M., D.L., S.S., M.K., H.E.S., and S.E.K. did the behavior experiments and analysis supervised by A.S. and C.M.P. J.C.T. and J.-H.H. provided reagents. M.A.B., A.S., and P.F.W. wrote the manuscript and P.F.W. supervised the overall project. We thank Maria Papapavlou for administrative assistance; Holly Wellington, Ann Lawler, Johnisha Witherspoon, and Charles Hawkins for assistance in generating the Shank3(+/ΔC) mice; Uejin Kim, Jasmin Harpe, Matt Jo, Pennson Wang, Dakim Gaines, Olivia Tong, Julia Wynne, and Eugenia Cho for help with behavioral testing and data handling; Ya-Xian Wang for help with the electron microscopy preparation. This work was supported by National Institute of Neurological Disorders and Stroke grant 5R01NS070301-02 (P.F.W.), National Institute of Mental Health Core grant 5P50MH084020-03 (P.F.W.), National 973 Basic Research Program of China 20009CB941400 (B.X.), R21HD065290 (C.M.P.), R01MH081164 (C.M.P.), Autism Speaks (C.M.P. and M.K.), The Autism Science Foundation (C.M.P. and H.S.), The Hartwell Foundation (C.M.P.), NIDCD Intramural Program (R.S.P.), and Weatherstone predoctoral fellowship from Autism Speaks (M.A.B.).

Received: November 12, 2010
Revised: February 3, 2011
Accepted: March 28, 2011
Published online: May 12, 2011

REFERENCES

Bear, M.F., Huber, K.M., and Warren, S.T. (2004). The mGluR theory of fragile X mental retardation. Trends Neurosci. *27*, 370–377.

Beneken, J., Tu, J.C., Xiao, B., Nuriya, M., Yuan, J.P., Worley, P.F., and Leahy, D.J. (2000). Structure of the Homer EVH1 domain-peptide complex reveals a new twist in polyproline recognition. Neuron *26*, 143–154.

Bonaglia, M.C., Giorda, R., Borgatti, R., Felisari, G., Gagliardi, C., Selicorni, A., and Zuffardi, O. (2001). Disruption of the ProSAP2 gene in a t(12;22)(q24.1;q13.3) is associated with the 22q13.3 deletion syndrome. Am. J. Hum. Genet. *69*, 261–268.

Brakeman, P.R., Lanahan, A.A., O'Brien, R., Roche, K., Barnes, C.A., Huganir, R.L., and Worley, P.F. (1997). Homer: a protein that selectively binds metabotropic glutamate receptors. Nature *386*, 284–288.

Condra, J.A., Neibergs, H., Wei, W., and Brennan, M.D. (2007). Evidence for two schizophrenia susceptibility genes on chromosome 22q13. Psychiatr. Genet. *17*, 292–298.

DeLisi, L.E., Shaw, S.H., Crow, T.J., Shields, G., Smith, A.B., Larach, V.W., Wellman, N., Loftus, J., Nanthakumar, B., Razi, K., et al. (2002). A genome-wide scan for linkage to chromosomal regions in 382 sibling pairs with schizophrenia or schizoaffective disorder. Am. J. Psychiatry *159*, 803–812.

Durand, C.M., Betancur, C., Boeckers, T.M., Bockmann, J., Chaste, P., Fauchereau, F., Nygren, G., Rastam, M., Gillberg, I.C., Anckarsäter, H., et al. (2007). Mutations in the gene encoding the synaptic scaffolding protein SHANK3 are associated with autism spectrum disorders. Nat. Genet. *39*, 25–27.

Ehlers, M.D. (2003). Activity level controls postsynaptic composition and signaling via the ubiquitin-proteasome system. Nat. Neurosci. *6*, 231–242.

Ferguson, J.N., Young, L.J., and Insel, T.R. (2002). The neuroendocrine basis of social recognition. Front. Neuroendocrinol. *23*, 200–224.

Gauthier, J., Champagne, N., Lafrenière, R.G., Xiong, L., Spiegelman, D., Brustein, E., Lapointe, M., Peng, H., Côté, M., Noreau, A., et al; S2D Team. (2010). De novo mutations in the gene encoding the synaptic scaffolding protein SHANK3 in patients ascertained for schizophrenia. Proc. Natl. Acad. Sci. USA *107*, 7863–7868.

Geschwind, D.H. (2008). Autism: many genes, common pathways? Cell *135*, 391–395.

Hayashi, M.K., Tang, C., Verpelli, C., Narayanan, R., Stearns, M.H., Xu, R.M., Li, H., Sala, C., and Hayashi, Y. (2009). The postsynaptic density proteins Homer and Shank form a polymeric network structure. Cell *137*, 159–171.

Huber, K.M., Gallagher, S.M., Warren, S.T., and Bear, M.F. (2002). Altered synaptic plasticity in a mouse model of fragile X mental retardation. Proc. Natl. Acad. Sci. USA *99*, 7746–7750.

Kanne, S.M., and Mazurek, M.O. (2010). Aggression in children and adolescents with ASD: Prevalence and risk factors. J. Autism Dev. Disord. Published online October 20, 2010. 10.1007/s10803-010-1118-4.

Kato, A., Rouach, N., Nicoll, R.A., and Bredt, D.S. (2005). Activity-dependent NMDA receptor degradation mediated by retrotranslocation and ubiquitination. Proc. Natl. Acad. Sci. USA *102*, 5600–5605.

Marshall, C.R., Noor, A., Vincent, J.B., Lionel, A.C., Feuk, L., Skaug, J., Shago, M., Moessner, R., Pinto, D., Ren, Y., et al. (2008). Structural variation of chromosomes in autism spectrum disorder. Am. J. Hum. Genet. *82*, 477–488.

Moessner, R., Marshall, C.R., Sutcliffe, J.S., Skaug, J., Pinto, D., Vincent, J., Zwaigenbaum, L., Fernandez, B., Roberts, W., Szatmari, P., and Scherer, S.W. (2007). Contribution of SHANK3 mutations to autism spectrum disorder. Am. J. Hum. Genet. *81*, 1289–1297.

Mohn, A.R., Gainetdinov, R.R., Caron, M.G., and Koller, B.H. (1999). Mice with reduced NMDA receptor expression display behaviors related to schizophrenia. Cell *98*, 427–436.

Nesslinger, N.J., Gorski, J.L., Kurczynski, T.W., Shapira, S.K., Siegel-Bartelt, J., Dumanski, J.P., Cullen, R.F., Jr., French, B.N., and McDermid, H.E. (1994). Clinical, cytogenetic, and molecular characterization of seven patients with deletions of chromosome 22q13.3. Am. J. Hum. Genet. *54*, 464–472.

Powell, C.M., and Miyakawa, T. (2006). Schizophrenia-relevant behavioral testing in rodent models: a uniquely human disorder? Biol. Psychiatry *59*, 1198–1207.

Rampon, C., Tang, Y.P., Goodhouse, J., Shimizu, E., Kyin, M., and Tsien, J.Z. (2000). Enrichment induces structural changes and recovery from nonspatial memory deficits in CA1 NMDAR1-knockout mice. Nat. Neurosci. *3*, 238–244.

Rapoport, J., Chavez, A., Greenstein, D., Addington, A., and Gogtay, N. (2009). Autism spectrum disorders and childhood-onset schizophrenia: clinical and biological contributions to a relation revisited. J. Am. Acad. Child Adolesc. Psychiatry *48*, 10–18.

Roussignol, G., Ango, F., Romorini, S., Tu, J.C., Sala, C., Worley, P.F., Bockaert, J., and Fagni, L. (2005). Shank expression is sufficient to induce functional dendritic spine synapses in aspiny neurons. J. Neurosci. *25*, 3560–3570.

Sebat, J., Lakshmi, B., Malhotra, D., Troge, J., Lese-Martin, C., Walsh, T., Yamrom, B., Yoon, S., Krasnitz, A., Kendall, J., et al. (2007). Strong association of de novo copy number mutations with autism. Science *316*, 445–449.

Szumlinski, K.K., Lominac, K.D., Kleschen, M.J., Oleson, E.B., Dehoff, M.H., Schwarz, M.K., Seeburg, P.H., Worley, P.F., and Kalivas, P.W. (2005). Behavioral and neurochemical phenotyping of Homer1 mutant mice: possible relevance to schizophrenia. Genes Brain Behav. *4*, 273–288.